Research Article | Vol. 30, No. 13 / 20 Jun 2022 / Optics Express 23828
Optics EXPRESS

# Adjustable converter of bound state in the continuum basing on metal-graphene hybrid metasurfaces

YIFAN CHEN,[1,2] ZEXU LIU,[1] YUKE LI,[1] ZHENGDA HU,[1,3] JINGJING WU,[1] AND JICHENG WANG[1,2,*]

[1]School of Science, Jiangnan University, Wuxi 214122, China
[2]State Key Laboratory of Millimeter Waves, Southeast University, Nanjing, 210096, China
[3]Key Laboratory of Quantum Information, University of Science and Technology of China, Chinese Academy of Sciences, Hefei 230026, China
[*]jcwang@jiangnan.edu.cn

**Abstract:** The bound state in the continuum (BIC) is widely applied to metamaterial study in order to obtain robust resonance and high quality (Q) factor. In this paper, we propose a metallic metasurface structure that can support double types of BICs, and acquire quasi-BIC state by restructuring each type with a specific approach. Electric field distribution is investigated to explore the physic mechanism behind the evolution of BICs. Moreover, we substitute structured graphene with corresponding metal counterparts. The promoted design is able to switch freely between BIC and quasi-BIC state even after the fabrication, as the graphene would convert from semiconductor-like to metal-like when increasing the Fermi level. Further exploration on electric field distribution demonstrates the metallicity difference between graphene and gold, which leads to the exotic phenomenon emerge on the proposed metal-graphene structure. Finally, the proposed metal-graphene structure is applied to a digital coding display through Fermi level regulating. Therefore, our work provides deep insights to the BIC metasurface investigation, and introduces a desirable improvement for current BIC metasurface design to achieve the free conversion between BIC and quasi-BIC states.



## 1. Introduction

With the rapid development of optical communication, it raises booming demand towards high-efficient optical devices, thus leading to the pursuing of high quality factor (Q factor) optical resonators. High-Q resonances show the robust interaction between the resonators and electromagnetic waves, giving rise to various applications including filters [1], nonlinear optics [2] and biological sensors [3]. One plausible way to achieve high quality factor is using an extraordinary physical phenomenon: The bound state in the continuum (BIC). Although this notion of BIC was first proposed by von Neumann and Wigner in quantum mechanics [4], later it has been verified in acoustic [5], electromagnetic and photonic [6] as a ubiquitous wave phenomenon. The ideal BIC would possess infinite lifetime and quality factor, and it can't be observed in spectrum because it confines the light perfectly without any radiation leaking out [7]. Ascribing to its fascinating property, BIC has created plenty of potential applications, such as lasers [8], gratings [9,10], vortex beam generators [11–14] and negative refraction [15]. Two major approaches are universally accepted to realize BIC: The first method is called symmetry-protect BIC, as a structure with specific symmetry mode while embedded into the continuum state with distinct symmetry classes would exhibit this kind of BIC, as long as the symmetry mismatch preserved [16,17]. Another type of BIC can be generated by tuning the structural parameters of the resonator, when the outgoing waves to the continuum couple into the

#462221 https://doi.org/10.1364/OE.462221
Journal © 2022 Received 27 Apr 2022; revised 3 Jun 2022; accepted 3 Jun 2022; published 15 Jun 2022

Optics EXPRESS

same radiation channel and completely cancel each other out through interference. Therefore, it is entitled "parameter-tuned BIC", which is also well known as "accidental BIC" [18,19].

The prosperity of metamaterials (MMs) and metasurface (MSs) indicate a bright future to electromagnetic and photonic industry, providing an innovative technique to manufacture optical devices. Lots of eye-catching phenomena and applications have been realized and confirmed based on MMs/MSs: negative refraction [20], perfect absorption [21,22], Dirac-semimetal material [23–26] and BIC in photonic crystal (PhC) [27,28]. As metamaterials offer a powerful platform for BIC researches, scientists begin to introduce perturbations into existing common BIC designs, which could turn the BIC state into a quasi-BIC state [29]. Unlike perfect BIC state, the quasi-BIC allows the bound state to couple with extended state and release radiation into the continuum, which makes it observable in the spectrum. Compared with general resonances, quasi-BICs remain extremely high quality factor that usually present in the form of Fano resonances [30,31]. As mentioned above, for the symmetry-protect BIC, breaking its specific symmetry mode to make it evolve into a quasi-BIC: simply removing or adding some parts of the original pattern totally breaks the in-plane $C_2$ symmetry [32–34], and the inversion symmetry of other structures can be destructed by giving slight rotation or deviation [35–37]. Similarly, tuning the structural parameters could lead to different interference conditions through the radiation continuum, thus turning an accidental BIC into a quasi-BIC while the symmetry mode of existing design reserved [38]. Most structures based on metallic metasurfaces have the same defect: once after the fabrication, the metasurface devices can only work under a single status, either BIC or quasi-BIC. To overcome this shortage, recent researches have tried overlapping metals on graphene, in order to achieve dynamic control between BIC and quasi-BIC state [39].

With the inspiration of previous studies, we propose a novel structure basing on the metallic (gold) metasurface which exhibits both two types of BIC. By either breaking the mirror symmetry or adjusting the geometry parameters, our model would evolve into the quasi-BIC state and presents slight Fano resonances within terahertz (THz) frequency domain. Next, we replace metallic perturbations with the designed graphene pattern of the respective structure. As graphene could switch between metal-like and dielectric-like by voltage regulation, the modified graphene model realizes dynamic converting ability from BICs to quasi-BICs, even the structure design being fixed, which is impossible for original metallic models. Moreover, we investigate the electromagnetic field distribution of the structure at certain frequencies, giving deep insights to the generation and evolution of quasi-BICs. Besides, we find exotic phenomena in the transmission spectra caused by difference between graphene and gold, which shows clearly on the electromagnetic field distribution images. A digital coding display is put forward based on the graphene-modified model, which achieves dynamic transmission switch within the range of 0.83-0.92 THz by regulating the Fermi level of graphene.

## 2. Model design and simulation result

Fig. 1(a) illustrates the three-dimensional schematic of the proposed model, while Fig. 1(b) gives the detail structural design of a single unit cell. The whole structure is fabricated on a Si substrate, and uses gold to form the metasurface on the upper surface. The unit cell is in shape of a square with length $P$, and the metal design could be divided into two main parts: a cross shape comprising two identical rectangular gold strips, and a gold disk which overlaps at the center of the cross.

Fig. 2 shows how the proposed metasurface design can be modified to support both types of BICs, and further adapt each type of BIC design into its graphene counterpart. Symmetry-protect BIC can be easily destroyed by removing part of the gold strip, thus breaking the $C_2$ symmetry of structure. Without breaking the in-plane symmetry mode, an accidental BIC can be reached when the diameter of gold disk is accurately tuned to a certain value. Furthermore, the corresponding altering parts are replaced by the structured graphene to accomplish free BIC converting function.

Optics EXPRESS

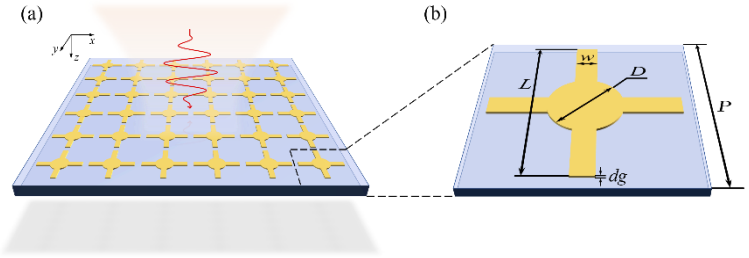


**Fig. 1.** (a) Three-dimensional schematic of proposed structure. (b) The whole structure uses Si as substrate with 8 μm thickness, and it is repeated by the same square unit cells with period $P$. The metallic MS is made of two identical rectangular gold strips with length $L$ and width $w$ which are placed orthogonally like a cross, and overlap a gold disk with diameter $D$ at the center of the cross. The thickness of gold is $dg$. Here $dg = 200$ nm, $L = 140$ μm, $w = 20$ μm, $P = 160$ μm, $D = 52$ μm.

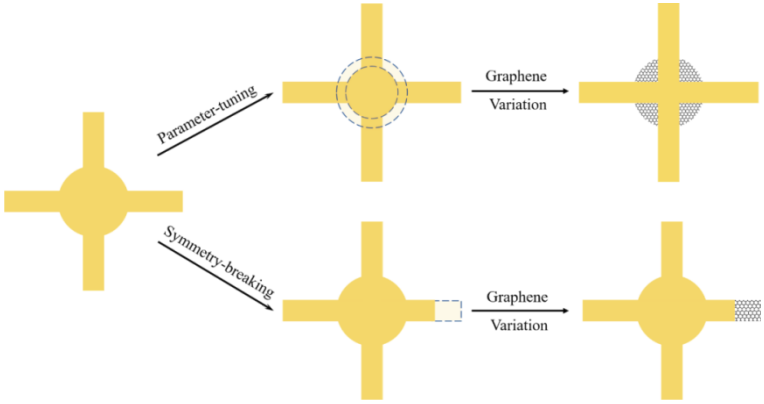


**Fig. 2.** The schematic of the original metallic metasurface design and its variation. The parameter-tuned BIC can be achieved by changing the diameter of metal disk at center, and decreasing the length of metal strip can break the symmetry-protect BIC. Finally,the structured graphene is placed below the corresponding designs to manufacture dynamic regulating BIC devices.

The temporal coupled-mode theory reveals the physical mechanism when two resonances are coupled into a single radiation channel, where the Hamiltonian of the resonator can be described as follow [40]:

$$H = \begin{pmatrix} \omega_1 & \kappa \\ \kappa & \omega_2 \end{pmatrix} - i \begin{pmatrix} \gamma_1 & \sqrt{\gamma_1\gamma_2} \\ \sqrt{\gamma_1\gamma_2} & \gamma_2 \end{pmatrix} \tag{1}$$

Here, $\kappa$ is near-field coupling term between two resonances, and $\omega_{1,2}$ stand for different resonant frequencies of the resonator, and $\gamma_{1,2}$ correspond to their radiation rate respectively. As two resonances coupled into the same channel, radiation via the continuum collapse ascribing to interference, thus $\sqrt{\gamma_1\gamma_2}$ represents the coupling term. Friedrich and Wintgen first analyzed the BIC condition if enough parameters are tuned [41]:

$$\kappa(\gamma_1 - \gamma_2) = \sqrt{\gamma_1\gamma_2}(\omega_1 - \omega_2) \tag{2}$$

Under this circumstance, one eigenvalue can become a pure real number, which indicates its corresponding eigenmode possesses no radiation decay and turns into the accidental-BIC state,

Optics EXPRESS

while the other mode would leak more radiation loss. Also, the BIC can be achieved when $\kappa = 0$ or $\gamma_1 = \gamma_2$ at the frequency where $\omega_1 = \omega_2$, or intuitively, two outgoing waves completely cancel each other out through interference.

Fig. 3(a) depicts the approach which the proposed model takes to reach the accidental-BIC, by tuning the structural parameters. Here the diameter $D$ of the metal disk becomes the only variable, and the incident plane wave is $y$-axis linear polarization.

The transmission spectra are listed in Fig. 3(b) as the disk diameter increased from 32 μm to 72 μm. When the diameter $D = 32$ μm, the MS supports with quasi-BIC states, where the leaking out radiation present in the form of Fano resonances at 1.52 THz and 1.66 THz, respectively. As the numerical value of diameter rising up, the Friedrich-Wintgen condition is met and those Fano resonances eventually vanish when $D = 52$ μm, forming a smooth curve in the transmission spectrum, which indicates an accident-BIC state of the model. Meanwhile, if the diameter keeps growing up to 72 μm, the structure would no longer satisfy the Friedrich-Wintgen condition, leading to the emergence of Fano peaks and the quasi-BIC state. It's succinct to investigate the evolution of the parameter-tuned BIC from the transmission spectra, but it can't figure the physical mechanism behind. Therefore, Fig. 4(a-f) are carried out showing how the change of diameter effects the interaction between the structure and electromagnetic field, and what happens when BICs convert into the quasi-BICs. Figure 4 (a) and (e) illustrate both electric field and electric field line distribution of the first and the second Fano dip when $D = 32$ μm, respectively. In this case, the structure possesses quasi-BIC features, and electromagnetic interaction is mainly constrained on the horizontal metal strip within a single unit. As the disk diameter gradually increasing to 52 μm, the vertical metal strip takes charge of most electric interaction, and the electric field lines connect adjacent metasurface units along $y$-axis, indicating a BIC state. If parameter $D$ continuously rising, eventually metal disk would restrict the majority of electric field and weaken the interaction between adjacent metal patterns, turning the device into quasi-BIC state.

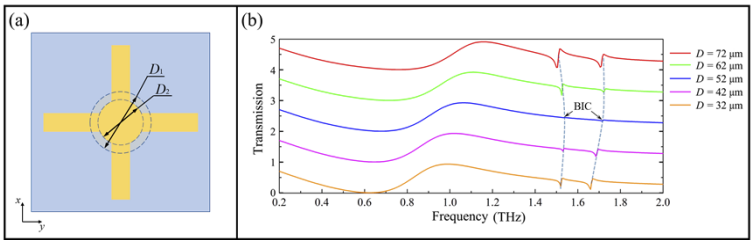


**Fig. 3.** The schematic of structure's accidental-BIC and its transmission spectra. (a) Diameter tuning of the proposed metasurface design, which introduces accidental-BIC to the model. (b) Transmission spectra of diameter variation, the evolution of BIC and the Fano resonance is depicted by the gray dash line.

To better illustrate the emergence of this BIC, the original design can be divided into separated mode, and Fig. 5(a) shows the transmission spectra of two separated parts. The cross mode possesses two Fano resonances at 1.52 THz and 1.66 THz, and the pure metal disk pattern also presents two Fano resonances around 1.6 THz. When the disk diameter gradually increases, the frequencies of its Fano resonances appear red-shifted, while the frequencies of cross mode remain unchanged. In Fig. 5(b) we further explore the electrical field distributions pictures of two modes. The electric field shows the opposite polarity in disk mode and cross mode at same location. Thus, when the disk diameter reaches 52 μm, the polarity of disk mode coincides with the cross mode and cause the interference of outgoing radiation, avoiding the simultaneous existence of two modes (anti-cross phenomenon) and forming a Friedrich-Wintgen BIC. Here in the electric

Optics EXPRESS

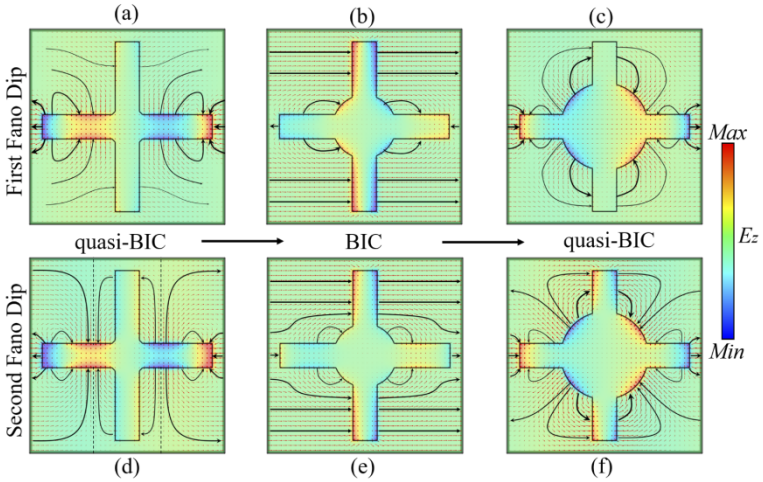


**Fig. 4.** Electric field ($E_z$) and electric field line distribution with disk diameter variation. First row shows the first Fano resonance around 1.52 THz; Second row shows the second Fano resonance around 1.66 THz. Small red arrows depict accurate azimuth of electric field line, and large black arrows represent the overall flow of electric field. The observing plane is set 0.5 μm below the MS plane. (a) $D = 32$ μm, $f = 1.52$ THz. (b) $D = 52$ μm, $f = 1.52$ THz. (c) $D = 72$ μm, $f = 1.52$ THz. (d) $D = 32$ μm, $f = 1.66$ THz. (e) $D = 52$ μm, $f = 1.70$ THz. (f) $D = 72$ μm, $f = 1.70$ THz.

field distributions, the cross mode become more lossy, and its metallic intrinsic radiation loss form a smooth curve of the transmission spectrum rather than zero transmission [42,43].

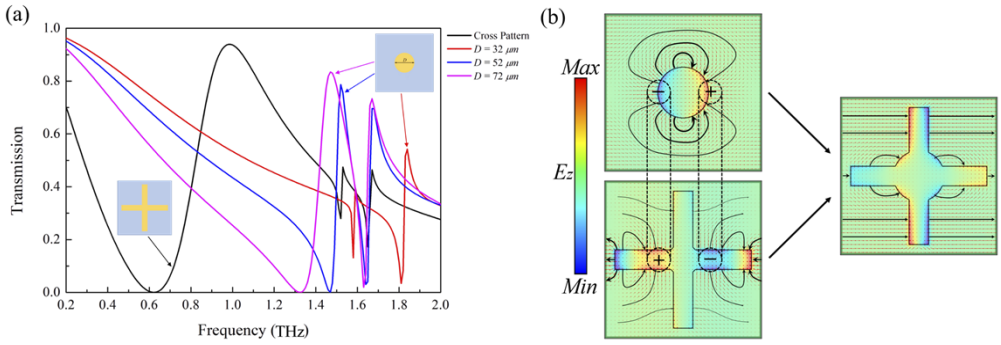


**Fig. 5.** (a) The transmission spectra for separated modes. The frequencies of Fano resonances of the disk mode present red-shifted when D increases. (b) The electric field distribution of two modes at first Fano resonance. The diameter of metal disk is 52 μm. The electric field of disk mode and cross mode present opposite polarity, thus when two pattern merged, the outgoing radiation would collapse to avoid simultaneous existence of two modes. The cross mode becomes more lossy, and its metallic intrinsic radiation loss form a smooth curve of the transmission spectrum.

The original MS designs also possess symmetry-protect BIC. By breaking the in-plane $C_2$ symmetry, the model would convert into a new quasi-BIC state. Figure 6(a) shows the way that structure breaks $C_2$ symmetry by cutting off partof the gold strip. The transmission spectra in Fig. 6(c-f) illustrate the evolution of BIC when the gap length g changes. When $g = 0$ μm, metasurface design possesses $C_2$ symmetry and forbids the outgoing radiation coupling between

Optics EXPRESS

different symmetry classes, thus forming a BIC state at 0.73 THz. Since introducing the gap, the structure no longer holds $C_2$ symmetry, leading to radiation coupling between distinct symmetry modes and quasi-BIC states. Therefore, a narrowband transmission peak can be found at 0.81 THz when $g = 20$ μm.

Electric field distribution of several prime frequencies is shown in Fig. 6(c-f). In Fig. 6(c), the structure preserves in-plane $C_2$ symmetry ($g = 0$ μm), thus, the device is working under BIC state at 0.73 THz. The z-direction electric field constrain on the vertical metal strip, and field lines simply end within a single unit. Figure 6(d) and (f) depict two quasi-BIC dips when $g = 20$ μm at 0.73 THz and 0.9 THz respectively, and both the electric field lines show strong constraint in one MS pattern. But for the quasi-BIC peak at 0.81 THz, which is shown in Fig. 6(e), the electric field line would attach to the metasurface patterns nearby, rather than end in the same unit. From these pictures we discover the phenomenon that the symmetry-protect BICs have: If the electromagnetic interaction is mainly restricted within single pattern, the model more likely possesses the bound state in the continuum; But if the electric field line mode presents strong connections between adjacent MS units, a quasi-BIC state will probably be activated. Which is distinct from the accidental BICs.

## 3. Graphene variation design and applications

With the purpose of achieving model's switching function, pre-designed graphene replaces the part of the original metal structure. Here, for each type of BIC, we propose its corresponding graphene promoted design: Fig. 7(a) shows the graphene-form of parameter-tuned BIC, which, in the previous investigation, is reached by altering disk diameter. So, in this case, the gold disk is completely replaced by the monolayer graphene roundel, and it is settled below the metal cross. A similar technique is utilized on symmetry-protect BIC, demonstrated by Fig. 7(b), while part of gold strip is removed and then substituted by graphene strips. Each improved model is expected to switch between different states as the bias voltage changes.

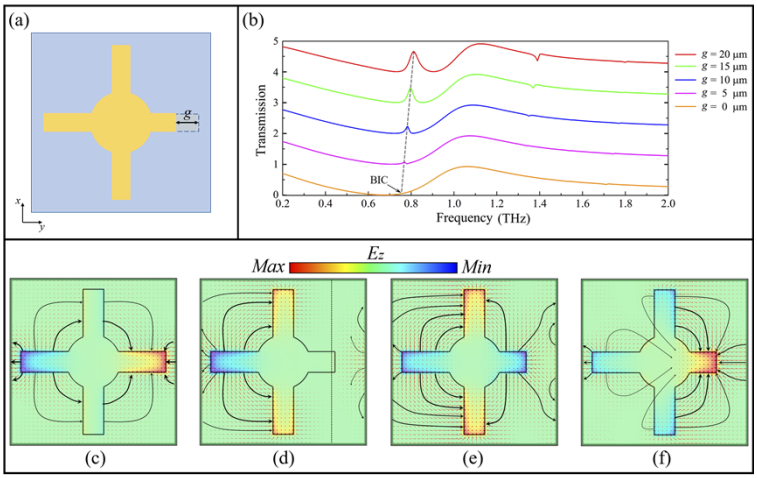


**Fig. 6.** (a) The symmetry is broken by introducing gap on the vertical gold strip, and the gap length is $g$. (b) The transmission spectrum changes as gap increasing, the evolution of BIC is depicted by the gray dash line. (c-f) Electric field (Ez) and electric field line distribution under symmetry breaking condition: (c) The symmetry-protect BIC, $g = 0$ μm, $f = 0.73$ THz. (d) The first quasi-BIC dip, $g = 20$ μm, $f = 0.73$ THz. The dash line indicates the boundary that no electric field line could pass through. (e) The quasi-BIC peak, $g = 20$ μm, $f = 0.81$ THz. (f) The second quasi-BIC dip, $g = 20$ μm, $f = 0.90$ THz.

Optics EXPRESS

The thickness of a monolayer graphene is about 0.34 nm, which is even far thinner than the thickness of metallic metasurface. Therefore, graphene is regarded as a perfect two-dimensional material with zero thickness, and it can be simulated by introducing surface current density. Kubo formula excellently describes the conductivity $\sigma$ of monolayer graphene, which contains interband and intraband electron transition contribution [44]:

$$\begin{aligned}\sigma_{gra} = \sigma_{inter} + \sigma_{intra} = \frac{2e^2 k_B T}{\pi\hbar^2}\frac{i}{\omega + i/\tau}\ln\left[2\cosh\left(\frac{E_f}{2k_B T}\right)\right] \\ + \frac{e^2}{4\hbar^2}\left[\frac{1}{2} + \frac{1}{\pi}\arctan\left(\frac{\hbar\omega - 2E_f}{2k_B T}\right) - \frac{i}{2\pi}\ln\frac{(\hbar\omega + 2E_f)^2}{(\hbar\omega - 2E_f)^2 + 4(k_B T)^2}\right]\end{aligned} \tag{3}$$

Here $k_B$, $\hbar$ and $e$ represent the Boltzmann constant, reduced Plank constant and electron charge, respectively. Giving the Kalvin temperature $T$ with room temperature $T = 300\ K$, $\omega$ stands for the angular frequency of the incident terahertz wave. $\tau$ is the electron-phonon relaxation time, and $E_f$ represents the graphene's Fermi energy level. The basic operating situation of the proposed model can satisfy the low concentration doping condition $E_f \gg \hbar\omega$ and $E_f \gg k_B T$. As a consequence, the Kubo formula is able to be simplified into Drude-like equation:

$$\sigma_{gra} = \frac{e^2 E_f}{\pi\hbar^2}\frac{i}{\omega + i/\tau} \tag{4}$$

where $\tau = \mu E_f/(e{v_F}^2)$, $v_F$ denotes the Fermi velocity of graphene with the value of $1\times10^6$ m·s$^{-1}$, and the media carrier mobility is $\mu = 10000$ cm$^2$V$^{-1}$s$^{-1}$. By changing the Fermi energy level $E_f$, graphene can present a considerable transformation from semiconductor-like to metal-like, thus supporting the switching ability of the promoted design.

Fig. 8 investigates transmission spectra of graphene variant corresponding to the parameter-tuned BIC. When the Fermi level $E_f = 0.01$ eV, graphene works under semiconductor-like status, thus, the Friedrich-Wintgen condition is unsatisfied and lead to Fano resonances at 1.42 THz and 1.58 THz. As the value of Fermi level increases, the Fano resonances gradually vanish, eventually entering the BIC state where $E_f = 0.8$ eV. If $E_f$ keeps rising to 1 eV, the model would turn into a quasi-BIC again, simultaneously the Fano resonances appear at 1.41 THz and 1.6 THz. Basically, the graphene variant shows analogical BIC evolution compared to its metal counterpart. Both designs can achieve BIC states at certain frequencies with proper parameters, whether excessive or insufficient adjusted parameters would result in the emergence of Fano resonances and quasi-BIC states.

From the electric field distribution pictures for the first and the second Fano dip in Fig. 8(c) and (e) respectively, where $E_f = 0.01$ eV, almost the same electric field line modes can be found in graphene variant and original metallic design (Fig. 4(a) and (d)). In this case, graphene doesn't interact much with the incident THz wave. While in Fig. 8(d) and (f), where $E_f = 0.8$ eV, the graphene pattern shows robust electric interaction compared with metal strips, which is far stronger than original gold disks. And electric field lines mainly travel along the $y$-axis, causing strong connections between adjacent units. Therefore, the suggested graphene-promoted design could convert from quasi-BIC states to BIC states by adjusting the Fermi level, which is controlled by external bias voltage.

So far, the graphene variant of parameter-tuned BIC shares a lot of similarities with the original structure, and it is convenient for us to further investigate its physic mechanism through contrasts. But when we adapt the symmetry-protect BIC into its graphene variation (see Fig. 9(a)), the difference between meta-like graphene and gold is magnified. Consequently, the transmission spectra in Fig. 9(b) present a few exotic phenomena. When $E_f = 0.01$ eV, the transmission spectrum resembles the original metal structure, but it is accompanied with frequency-shifting. As the Fermi level raises, the frequency of first quasi-BIC dip basically remains unchanged, while the second dip's frequency experiences a great blue-shifted. Thus, the quasi-BIC peak between

Optics EXPRESS

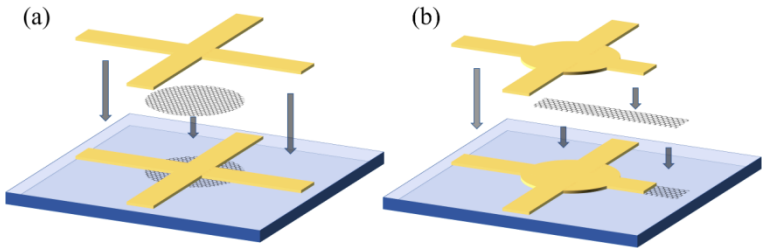


**Fig. 7.** (a) The graphene variation of parameter-tuned BIC. The thickness of Si substrate is 8 μm. The above gold cross has identical geometry parameters ($L = 140$ μm, $w = 20$ μm, $dg = 200$ nm), and the diameter of graphene roundel is 52 μm. (b) The graphene variation of symmetry-protect BIC. Above gold pattern's geometry parameters are $L = 140$ μm, $w = 20$ μm, $D = 52$ μm, $dg = 200$ nm, $g = 20$ μm, and the graphene strip overlaps below is rectangle with identical length $L = 140$ μm and width $w = 20$ μm.

two dips seems being extended, forming a broadband high transmission peak. Although the initial purpose is making the transmission spectrum identical when graphene presents metal-like status, two quasi-BIC dip modes exist even we elevate graphene's Fermi level to its physical limit. At 0.85 THz, the transmissivity of proposed design varies from 1% to 78% when the Fermi level increases from 0.01 eV to 1 eV.

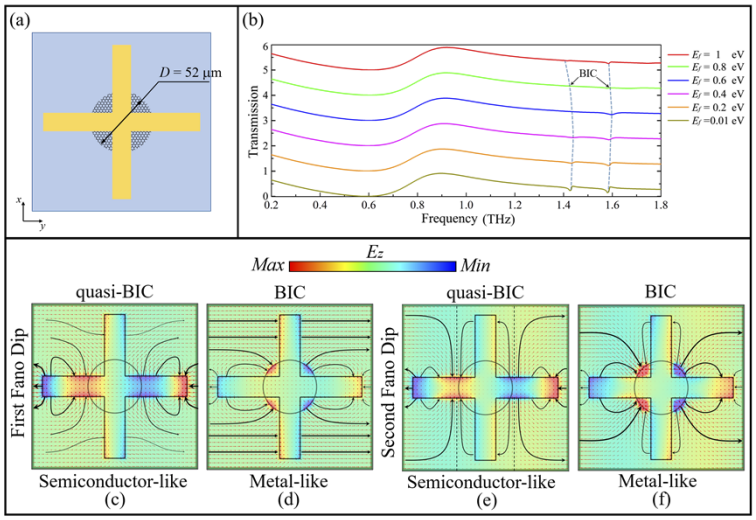


**Fig. 8.** (a) The graphene variation of parameter-tuned BIC on the single unit cell. The metal disk is replaced by the graphene roundel which is placed under metal cross. (b) The transmission spectra when the Fermi level increases, and the evolution of BIC and Fano resonances are depicted by the gray dash line. (c-f) Electric field ($Ez$) and electric field line distribution with the graphene variation of parameter-tuned BICs: (c) $E_f = 0.01$ eV, $f = 1.42$ THz. (d) $E_f = 0.8$ eV, $f = 1.42$ THz. (e) $E_f = 0.01$ eV, $f = 1.58$ THz. (f) $E_f = 0.8$ eV, $f = 1.58$ THz.

We further explore the electric field mode at 0.85 THz when the value of Fermi level equals to 0.01 eV and 1 eV, respectively. In Fig. 10, it's clear when $E_f = 0.01$ eV the electric field mode resembles the original metal design (in Fig. 6(d)), meaning the graphene is working under the semiconductor condition and doesn't take part in the electromagnetic interaction. When $E_f$ increases, graphene gradually becomes metal-like status, but the difference of metallicity between

Optics EXPRESS

graphene and gold splits the electric field lines apart. The graphene captures many electric field lines and thus weakens the interaction between adjacent patterns, and this phenomenon remains even when the Fermi level reaches 1 eV. When $E_f = 1$ eV, graphene presents stronger metallicity and tries to form a complete metal strip without gaps, and the electric field lines mainly travel along $y$-axis.

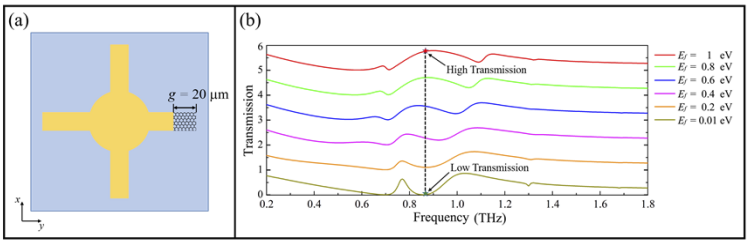


**Fig. 9.** (a) The graphene variation of symmetry-protect BIC in a single unit cell. The rectangle graphene strip is placed under the symmetry-broken metasurface structre. (b) The transmission spectra as the Fermi level increasing. The black dash line locates at 0.85THz, where the transmission changes magnificently from 1% to 78%.

Therefore, within the frequency domain indicated by blue shaded zone, the transmission value undergoes a considerable change when Fermi level varies. Inspired by that, we could adapt the model into dynamic controlled transmission devices, which can be applied to digital display or optical switch. The flow-process diagram of the applied digital display device is listed on Fig. 11(a). First, the input image is divided into the same pixel size as the number of metasurface units, in order to form a digital coding signal for bias voltage control. Then, according to the digital coding signal, the corresponding graphene unit is switched into a high/low transmission state, when the frequency of the incident wave source ranges within 0.83-0.92 THz, we can obtain a clear output image on the display plane. Through regulating the digital coding signal, the output image also varies freely.

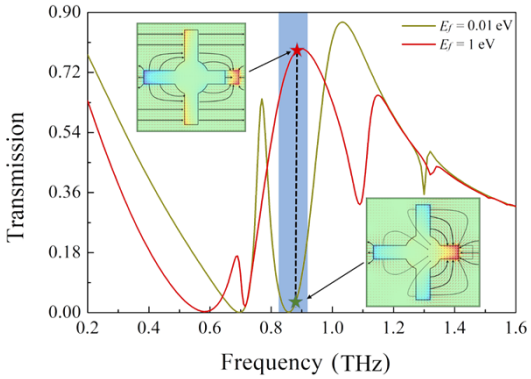


**Fig. 10.** The detail spectra information and electric field distribution of graphene variant. The black dash line locates at 0.85THz and two stars stand for the corresponding points when $E_f$ increases. Blue shaded area (0.83-0.92THz) denotes the frequency domain that can be utilized for dynamic controlled transmission.

Optics EXPRESS

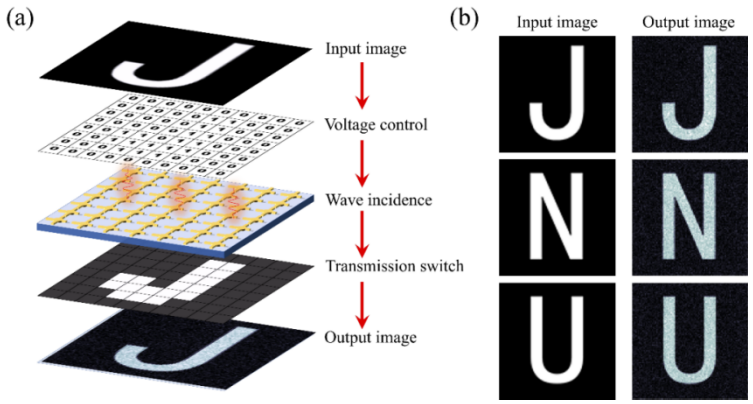


**Fig. 11.** (a)The flow-process chart of proposed dynamic digital display. The frequency of backlight source ranges within the blue shaded zone (0.83-0.92THz) depicted in Fig. 10. (b) The simulation result of output image exhibited by the proposed dynamic digital display.

## 4. Conclusion

In summary, we propose an innovative gold metasurface structure that can support both parameter-tuned BIC and symmetry-protect BIC. Two Fano resonances vanish and appear through tuning the diameter of gold disk, indicating the model switching from BIC state to quasi-BIC state. A narrowband transmission peak emerges as we introduce a gap into the metal strip, because the existence of gap breaks the in-plane $C_2$ symmetry, changing symmetry-protect BICs into quasi-BICs. Further investigation on electric field distribution and electric field line mode gives us the physical mechanism behind. If the electromagnetic interaction is mainly restricted within a single pattern, the model more likely possesses the bound state in the continuum; If the electric field line mode presents strong connections between adjacent MS units, the model probably enters a quasi-BIC state. Moreover, we adapt the original structure to its graphene variants, purposing on achieving the function of dynamic conversion. Gold disk is replaced by a graphene roundel in the variant of parameter-tuned BICs, and structure can freely convert from quasi-BIC states to BIC states by adjusting the Fermi level. In the variation of symmetry-protect BIC, a broadband transmission peak is investigated at the high Fermi level, while the pictures of electric field demonstrate the metallicity difference between graphene and gold, which explains the reason two quasi-BIC dips persist. Utilizing the low-high transmission change around 0.85 THz, we put forward a digital display which is coded and regulated by the Fermi level of graphene-metal metasurface.

**Funding.** National Natural Science Foundation of China (11811530052, 1211101294); Intergovernmental Science and Technology Regular Meeting Exchange Project of Ministry of Science and Technology of China (CB02-20); Open Fund of State Key Laboratory of Millimeter Waves (K202105, K202238); State Key Laboratory of Millimeter Waves (KQI201); Undergraduate Research and Innovation Projects of China (2021102Z).

**Disclosures.** The authors declare no conflicts of interest.

**Data availability.** The data that support the findings of this study are available from the corresponding author upon reasonable request.

## References

1. D. R. Abujetas, A. Barreda, F. Moreno, A. Litman, J. M. Geffrin, and J. A. Sánchez-Gil, "High-Q transparency band in all-dielectric metasurfaces induced by a quasi bound state in the continuum," Laser & Photonics Reviews **15**(1), 2000263 (2021).
2. K. Koshelev, S. Kruk, M. G. Elizaveta, J. H. Choi, A. Bogdanov, H. G. Park, and Y. Kivshar, "Subwavelength dielectric resonators for nonlinear nanophotonics," Science **367**(6475), 288–292 (2020).

Optics EXPRESS


3. M. S. Luchansky and R. C. Bailey, "High-Q optical sensors for chemical and biological analysis," Anal. Chem. **84**(2), 793–821 (2012).
4. J. V. Neumann and E. Wigner, "Über merkwürdige diskrete Eigenwerte," Phys. Z. **30**(524), 291–293 (1929).
5. N. A. Cumpsty and D. S. Whitehead, "The excitation of acoustic resonances by vortex shedding," Journal of Sound and Vibration **18**(3), 353–369 (1971).
6. C. W. Hsu, B. Zhen, J. Lee, S. L. Chua, S. G. Johnson, J. D. Joannopoulos, and M. Soljačić, "Observation of trapped light within the radiation continuum," Nature **499**(7457), 188–191 (2013).
7. C. W. Hsu, B. Zhen, A. D. Stone, J. D. Joannopoulos, and M. Soljačić, "Bound states in the continuum," Nat. Rev. Mater. **1**(9), 16048 (2016).
8. S. T. Ha, H. F. Yuan, N. K. Emani, Z. Y. Pan, R. M. Bakker, P. D. Ramon, I. Arseniy, and I. Kuznetsov, "Directional lasing in resonant semiconductor nanoantenna arrays," Nat. Nanotechnol. **13**(11), 1042–1047 (2018).
9. J. M. Foley, S. M. Young, and J. D. Phillips, "Symmetry-protected mode coupling near normal incidence for narrow-band transmission filtering in a dielectric grating," Phys. Rev. B: Condens. Matter Mater. Phys. **89**(16), 165111 (2014).
10. X. F. Yin, J. C. Jin, M. Soljačić, C. Peng, and B. Zhen, "Observation of topologically enabled unidirectional guided resonances," Nature **580**(7804), 467–471 (2020).
11. B. Zhen, C. W. Hsu, L. Lu, A. D. Stone, and M. Soljačić, "Topological Nature of Optical Bound States in the Continuum," Phys. Rev. Lett. **113**(25), 257401 (2014).
12. Y. W. Zhang, A. Chen, W. Z. Liu, C. W. Hsu, B. Wang, F. Guan, X. H. Liu, L. Shi, L. Lu, and J. Zi, "Observation of Polarization Vortices in Momentum Space," Phys. Rev. Lett. **120**(18), 186103 (2018).
13. B. Wang, W. Z. Liu, M. X. Zhao, J. J. Wang, Y. W. Zhang, A. Chen, F. Guan, X. H. Liu, L. Shi, and J. Zi, "Generating optical vortex beams by momentum-space polarization vortices centred at bound states in the continuum," Nat. Photonics **14**(10), 623–628 (2020).
14. T. R. Bai, Q. Li, Y. Q. Wang, Y. F. Chen, Z. D. Hu, and J. C. Wang, "Terahertz vortex beam generator based on bound states in the continuum," Opt. Express **29**(16), 25270–25279 (2021).
15. Z. Y. Zhang, F. F. Qin, Y. Xu, S. N. Fu, Y. C. Wang, and Y. W. Qin, "Negative refraction mediated by bound states in the continuum," Photonics Res. **9**(8), 1592–1597 (2021).
16. R. Ulrich, "Modes of propagation on an open periodic waveguide for the far infrared," Symposium on Optical and Acoustical Micro-Electronics, 359–376 (1975).
17. J. Lee, B. Zhen, S. L. Chua, W. Qiu, J. D. Joannopoulos, M. Soljačić, and O. Shapira, "Observation and differentiation of unique high-Q optical resonances near zero wave vector in macroscopic photonic crystal slabs," Phys. Rev. Lett. **109**(6), 067401 (2012).
18. K. Koshelev, A. Bogdanov, and Y. Kivshar, "Meta-optics and bound states in the continuum," Sci. Bull. **64**(12), 836–842 (2019).
19. M. V. Rybin, K. L. Koshelev, Z. F. Sadrieva, K. B. Samusev, A. A. Bogdanov, M. F. Limonov, and Y. S. Kivshar, "High-Q supercavity modes in subwavelength dielectric resonators," Phys. Rev. Lett. **119**(24), 243901 (2017).
20. V. M. Shalaev, "Optical negative-index metamaterials," Nat. Photonics **1**(1), 41–48 (2007).
21. H. J. Li, C. S. Ji, Y. Z. Ren, J. G. Hu, M. Qin, and L. L. Wang, "Investigation of multiband plasmonic metamaterial perfect absorbers based on graphene ribbons by the phase-coupled method," Carbon **141**, 481–487 (2019).
22. Y. F. Chen, X. S. Pan, Z. Y. Bao, Y. Q. Wang, Z. D. Hu, and J. C. Wang, "Tunable Terahertz Perfect Absorbers With Dual Peak Based on Reverse Graphene Patch Metamaterials," IEEE Photonics J. **13**(3), 1–12 (2021).
23. X. He, F. Liu, F. Lin, and W. Shi, "Tunable terahertz Dirac semimetal metamaterials," J. Phys. D: Appl. Phys. **54**(23), 235103 (2021).
24. J. Leng, J. Peng, A. Jin, D. Cao, D. Liu, X. He, and F. Liu, "Investigation of terahertz high Q-factor of all-dielectric metamaterials," Opt. Laser Technol. **146**, 107570 (2022).
25. X. He, F. Lin, F. Liu, and W. Shi, "Tunable terahertz Dirac-semimetal hybrid plasmonic waveguides," Opt. Mater. Express **12**(1), 73–84 (2022).
26. X. He, F. Liu, F. Lin, and W. Shi, "3D Dirac Semimetal Supported Tunable TE Modes," Ann. Phys. **534**(4), 2100355 (2022).
27. W. M. Ye, Y. Gao, and J. L. Liu, "Singular Points of Polarizations in the Momentum Space of Photonic Crystal Slabs," Phys. Rev. Lett. **124**(15), 153904 (2020).
28. Y. X. Zeng, G. W. Hu, K. P. Liu, Z. X. Tang, and C. W. Qiu, "Dynamics of Topological Polarization Singularity in Momentum Space," Phys. Rev. Lett. **127**(17), 176101 (2021).
29. M. Rybin and Y. Kivshar, "Supercavity lasing," Nature **541**(7636), 164–165 (2017).
30. F. Zhang, X. Huang, Q. Zhao, L. Chen, Y. Wang, Q. Li, X. He, C. Li, and K. Chen, "Fano resonance of an asymmetric dielectric wire pair," Appl. Phys. Lett. **105**(17), 172901 (2014).
31. W. X. Lim and R. Singh, "Universal behaviour of high-Q Fano resonances in metamaterials: Terahertz to near-infrared regime," Nano Convergence **5**(1), 1–7 (2018).
32. V. A. Fedotov, M. Rose, S. L. Prosvirnin, N. Papasimakis, and N. I. Zheludev, "Sharp trapped-mode resonances in planar metamaterials with a broken structural symmetry," Phys. Rev. Lett. **99**(14), 147401 (2007).
33. P. P. Vabishchevich, S. Liu, M. B. Sinclair, G. A. Keeler, G. M. Peake, and I. Brener, "Enhanced second-harmonic generation using broken symmetry III-V semiconductor Fano metasurfaces," ACS Photonics **5**(5), 1685–1690 (2018).

Optics EXPRESS


34. D. R. Abujetas, N. V. Hoof, S. T. Huuren, J. G. Rivas, and J. A. Sánchez-Gil, "Spectral and temporal evidence of robust photonic bound states in the continuum on terahertz metasurfaces," Optica **6**(8), 996–1001 (2019).
35. K. Koshelev, S. Lepeshov, M. K. Liu, A. Bogdanov, and Y. Kivshar, "Asymmetric Metasurfaces with High-Q Resonances Governed by Bound States in the Continuum," Phys. Rev. Lett. **121**(19), 193903 (2018).
36. V. R. Tuz, V. V. Khardikov, A. S. Kupriianov, K. L. Domina, S. Xu, H. Wang, and H. B. Sun, "High-quality trapped modes in all-dielectric metamaterials," Opt. Express **26**(3), 2905–2916 (2018).
37. S. Han, P. Prakash, W. H. Wang, Y. K. Srivastava, M. V. Rybin, and R. Singh, "Extended bound states in the continuum with symmetry-broken terahertz dielectric metasurfaces," Adv. Opt. Mater. **9**(7), 2002001 (2021).
38. X. G. Zhao, C. X. Chen, K. Kaj, I. Hammock, Y. W. Huang, R. D. Averitt, and X. Zhang, "Terahertz investigation of bound states in the continuum of metallic metasurfaces," Optica **7**(11), 1548–1554 (2020).
39. J. T. Li, J. Li, C. L. Zheng, Z. Yue, S. L. Wang, M. Y. Li, H. L. Zhao, Y. T. Zhang, and J. Q. Yao, "Free switch between bound states in the continuum (BIC) and quasi-BIC supported by graphene-metal terahertz metasurfaces," Carbon **182**, 506–515 (2021).
40. S. Fan, W. Suh, and J. D. Joannopoulos, "Temporal coupled-mode theory for the Fano resonance in optical resonators," J. Opt. Soc. Am. A **20**(3), 569–572 (2003).
41. H. Friedrich and D. Wintgen, "Interfering resonances and bound states in the continuum," Phys. Rev. A. **32**(6), 3231–3242 (1985).
42. M. Kang, S. Zhang, M. Xiao, and H. Xu, "Merging bound states in the continuum at off-high symmetry points," Phys. Rev. Lett. **126**(11), 117402 (2021).
43. S. I. Azzam, V. M. Shalaev, A. Boltasseva, and A. V. Kildishev, "Formation of bound states in the continuum in hybrid plasmonic-photonic systems," Phys. Rev. Lett. **121**(25), 253901 (2018).
44. L. A. Falkovsky and S. S. Pershoguba, "Optical far-infrared properties of a graphene monolayer and multilayer," Phys. Rev. B: Condens. Matter Mater. Phys. **76**(15), 153410 (2007).